Anisotropic Friedel oscillations in a two-dimensional electron gas with a Rashba–Dresselhaus spin–orbit interaction

I. V. Kozlov, and Yu. A. Kolesnichenko

Citation: Low Temperature Physics **43**, 855 (2017); doi: 10.1063/1.4995636
View online: http://dx.doi.org/10.1063/1.4995636
View Table of Contents: http://aip.scitation.org/toc/ltp/43/7
Published by the American Institute of Physics

LOW TEMPERATURE PHYSICS VOLUME 43, NUMBER 7 JULY 2017

Anisotropic Friedel oscillations in a two-dimensional electron gas with a Rashba–Dresselhaus spin–orbit interaction

I. V. Kozlov and Yu. A. Kolesnichenko[a)]

B. Verkin Institute for Low Temperature Physics and Engineering, National Academy of Science of Ukraine, Kharkiv 61103, Ukraine

(Submitted February 17, 2017)
Fiz. Nizk. Temp. **43**, 1067–1079 (July 2017)

We present a theoretical study of the spatial distribution of the local density of states (LDOS) and the local magnetization density (LMD) in the vicinity of a magnetic point-defect in a degenerate two-dimensional electron gas with a mixed Rashba-Dresselhaus spin-orbit coupling interaction (SOI). The dependence of the Friedel oscillations, which arise under these conditions, on the ratio of the SOI constants is investigated. We obtain asymptotic expressions for the oscillatory parts of the LDOS and the LMD, that are accurate for large distances from the defect. It is shown, that the Friedel oscillations are significantly anisotropic and contain several harmonics for certain ratios of the SOI constants. Period of the oscillations for directions along the symmetry axes of the Fermi contours are determined. Finally, we introduce a method for determining the values of the two SOI constants by measuring the period of the Friedel oscillations of the LDOS and the LMD for different harmonics. *Published by AIP Publishing.* [http://dx.doi.org/10.1063/1.4995636]

1. Introduction

In two-dimensional (2D) electronic systems, such as 2D electronic gasses in quantum wells or 2D surface states, the spin-orbit interaction (SOI) leads to a dependence of the spin direction on the direction of the wavevector **k** (see Ref. 1) This leads to the SOI having an influence on the electron-defect interactions. Backscattering from non-magnetic impurities is significantly reduced in the presence of SOI,[2] while additional scattering channels can become allowed in the presence of magnetic impurities.[3] These properties influence conductivity and magnetoresistance of 2D systems, making electron scattering from impurities in the presence of SOI, a particularly interesting subject.

Friedel oscillations[4,5] of the electron density near impurities are one of the clearest signs of the quantum nature of scattering, caused by the interference and reflection of the electronic waves from impurities. Oscillations in the electron gas magnetization, having a similar physical nature to the Friedel oscillations (see for example Ref. 7), arise above the Kondo temperature or during electron scattering from an incompletely screened magnetic impurity with a magnetic moment $S \geq 1$.[6] It is worth noting that compared to the seminal work of Friedel,[4] where the oscillations in the local density of the electrons $\Delta n_{osc}(\epsilon_F, r)$ were studied as a function of the distance from the defect, r ($\Delta n_{osc} \propto r^{-2}$ in the 2D case), the oscillations of the local density of states (LDOS) $\Delta\rho_{osc}(\epsilon, \mathbf{r}) = \partial\Delta n_{osc}(\epsilon, \mathbf{r})/\partial\epsilon$ at energy ϵ equal to the Fermi energy, decay much more slowly with distance from the defect ($\Delta n_{osc} \propto r^{-1}$ in the 2D case). LDOS oscillations at the Fermi level are often called Friedel-like oscillations.[8] Consistent with modern literature,[9] we use the term "Friedel oscillations" when dealing with spatial oscillations in the LDOS and the oscillations in the local magnetization density (LMD) at $\epsilon = \epsilon_F$.

Observation and investigation of the Friedel oscillations of LDOS and LMD have been made possible by the advances in scanning tunneling microscopy (STM)[10] and spin-polarized scanning tunneling microscopy (SP-STM).[11] The spherical contact model of Tersoff and Hamann,[12] as well as the flat, inhomogeneous potential model of Kulik *et al.*[13] account for electron tunneling through extremely small areas. The latter turned out to be especially effective when taking into account the under-the-surface point-defects.[14,15] Both approaches lead to the same expression[16,17] for the measured SP–STM tunneling current

$$I_{SP-STM}(\mathbf{r}) \propto \rho_t\rho(\mathbf{r}) + \mathbf{M}_t\mathbf{M}(\mathbf{r}),$$

where $\rho(\mathbf{r})$ is the local density of electronic states and $\mathbf{M}(\mathbf{r})$ is the local density of the sample magnetization at a point $\mathbf{r}$ underneath the STM contact, whose density of states and density of magnetization are ρ_t and $\mathbf{M}_t$ respectively.

A significant number of works are dedicated to theoretical[10–16] and experimental[17–19] investigations of the oscillating dependence of the LDOS in the vicinity of a point defect in a 2D electron gas with a Rashba SOI.[20,21] It was shown that although scattering from a magnetic impurity accompanied by a spin-flip, does open additional electron backscattering channels, it does not influence the inhomogeneous LDOS distribution.[11,12] The same result[12] was obtained for the Dresselhaus SOI.[22] Works[11,12] predict that is possible to determine the SOI constant from the period of the LDOS spatial oscillations.

A series of experiments (see for example, review Ref. 23) suggest that certain conditions facilitate a combined, Rashba–Dresselhaus SOI (R-D SOI). In contrast to 2D systems with only a single type of SOI (Rashba or Dresselhaus), where spin-split Fermi-contours (FC) assume a circular shape, systems with R-D SOI exhibit an anisotropic dispersion relation. This imparts a significant influence on all electronic characteristics of the system. Beatings of the Friedel oscillations[24] and the existence of directionally enhanced electron currents[25] were predicted on this basis.

The present manuscript is framed in the Born-Oppenheimer approximation and investigates the spatial anisotropy of the LDOS and the LMD oscillations around a point defect having a partially screened magnetic moment **J**, oriented at an arbitrary angle with respect to the plane of the 2D electron gas with a R-D SOI. We obtain asymptotic expressions for the LDOS and the LMD, for directions coinciding with the FC symmetry axes, that are valid for distances from the defect that are much larger than the de Broglie electron wavelength. It is shown that the periods of the Friedel oscillations allow determination of the R-D SOI constant.

2. Problem formulation

2.1. System Hamiltonian

We start with a 2D electron gas, described by a Hamiltonian (see for example Ref. 26)

$$\hat{H}(\mathbf{k}) = \frac{\hbar^2 \hat{k}^2}{2m} + \alpha(\hat{\sigma}_x \hat{k}_y - \hat{\sigma}_y \hat{k}_x) + \beta(\hat{\sigma}_x \hat{k}_x - \hat{\sigma}_y \hat{k}_y), \quad (1)$$

where $\hat{\mathbf{k}} = -i\nabla$, m is the effective electron mass, $\hat{\sigma}_i$ are the Pauli matrices, α and β are the Rashba and Dresselhaus SOI constants, respectively. We assume that the spin-orbital interaction constants are positive ($\alpha, \beta > 0$).

Solving the Schrodinger equation yields the eigenvalues and the eigenfunctions of the Hamiltonian (1)

$$\epsilon_{1,2} = \frac{\hbar^2 k^2}{2m} \pm \sqrt{k^2(\alpha^2 + \beta^2) + 4\alpha\beta k_x k_y}, \quad (2)$$

$$\hat{\psi}_{1,2}(\boldsymbol{\rho}) = \frac{1}{2\pi\sqrt{2}} e^{i\mathbf{k}\boldsymbol{\rho}} \hat{\varphi}_{1,2}(\theta); \quad \hat{\varphi}_{1,2}(\theta) = \begin{pmatrix} e^{i\theta/2} \\ \pm e^{-i\theta/2} \end{pmatrix};$$
$$\operatorname{tg}\theta = \frac{\alpha k_x + \beta k_y}{\alpha k_y + \beta k_x}. \quad (3)$$

The spin part $\hat{\varphi}_{1,2}(\theta)$ of the wavefunction (3) satisfies the following relations:

$$\hat{\varphi}^\dagger_{1,2}(\theta)\hat{\varphi}_{1,2}(\theta) = 1; \quad \hat{\varphi}^\dagger_{1,2}(\theta)\hat{\varphi}_{2,1}(\theta) = 0;$$
$$\hat{\varphi}^\dagger_{1,2}(\theta)\hat{\varphi}_{1,2}(\theta+\pi) = 0; \quad \hat{\varphi}^\dagger_{1,2}(\theta)\hat{\varphi}_{2,1}(\theta+\pi) = -1. \quad (4)$$

The interaction of the electron with the magnetic defect, located at the point $\boldsymbol{\rho}_0$, is modeled with a two-dimensional potential

$$\hat{D}(\boldsymbol{\rho}) = \left(\gamma\hat{\sigma}_0 + \frac{1}{2}\mathbf{J}\hat{\boldsymbol{\sigma}}\right)\delta(\boldsymbol{\rho} - \boldsymbol{\rho}_0), \quad (5)$$

where $\boldsymbol{\rho}$ is the two-dimensional coordinate vector in the xy plane; γ is the constant of the electron-defect interaction, $\hat{\boldsymbol{\sigma}} = (\hat{\sigma}_x, \hat{\sigma}_y, \hat{\sigma}_z)$ is the Pauli vector, $\hat{\sigma}_0$ is a 2×2 identity matrix, $\mathbf{J}$ is the effective magnetic moment of the defect. We assume the direction of $\mathbf{J}$ to be fixed and will not consider processes involving flipping or precession of the defect spin.

2.2. Curvature of the isoenergetic contours

The energies in (2) correspond to two FCs $k = k_{1,2}(f, \epsilon_F)$:

$$k_{1,2}(f, \epsilon_F) = \mp\frac{m}{\hbar^2}\sqrt{\alpha^2 + \beta^2 + 2\alpha\beta\sin(2f)} + \sqrt{\frac{2m\epsilon_F}{\hbar^2} + \left(\frac{m}{\hbar^2}\right)^2\left[\alpha^2 + \beta^2 + 2\alpha\beta\sin(2f)\right]}, \quad (6)$$

where $\epsilon_F > 0$ is the Fermi energy and the angle, f determines the direction of the 2D wavevector $\mathbf{k}$

$$k_x = k\cos f; \quad k_y = k\sin f. \quad (7)$$

The spin part of the wavefunction (3) allows the determination of the relation between the spin directions $\mathbf{s}_{1,2}$ at each contour and the wavevector direction (7)

$$\mathbf{s}_{1,2} = \hat{\varphi}^\dagger_{1,2}(\theta)\boldsymbol{\sigma}\hat{\varphi}_{1,2}(\theta) = \pm(\sin\theta, -\cos\theta, 0). \quad (8)$$

It is known,[23] that under certain ratios of the R-D SOI constants, the larger (outer) FC $k = k_2(f, \epsilon_F)$ becomes non-convex, whereas the smaller (inner) contour $k = k_1(f, \epsilon_F)$ always shows a positive curvature $K_1(f, \epsilon_F) > 0$ (see Fig. 1),

$$K_i(f) = \frac{-k_i(f)k_i''(f) + 2k_i'(f)^2 + k_i(f)^2}{\left(k_i'(f)^2 + k_i(f)^2\right)^{3/2}}, \quad i = 1, 2. \quad (9)$$

From simple symmetry considerations of the $k_2(f, \epsilon_F)$ FC, it is apparent that the critical values of the SOI constants, corresponding to the onsets of concavity, occur when the curvature of the contour becomes zero, $K_1(f, \epsilon_F) = 0$ along the $k_x = -k_y$, $f = 3\pi/4, -\pi/4$ symmetry axes

$$K_{1,2}(f)|_{f=3\pi/4,-\pi/4} = \frac{|a-b|\sqrt{(a-b)^2+1} \pm 4ab}{k_F|a-b|\sqrt{(a-b)^2+1}\left(\sqrt{(a-b)^2+1} \mp |a-b|\right)}, \quad (10)$$

where $k_F = \sqrt{2m\epsilon_F}/\hbar$. Here and going forth we use the following dimensionless constants

$$a = \frac{m\alpha}{\hbar^2 k_F}, \quad b = \frac{m\beta}{\hbar^2 k_F}, \quad \kappa_{1,2} = \frac{k_{1,2}}{k_F} = \kappa_F \mp \kappa_0,$$
$$\kappa_F = \sqrt{1 + a^2 + b^2 + 2ab\sin(2f)}, \quad (11)$$
$$\kappa_0 = \sqrt{a^2 + b^2 + 2ab\sin(2f)}.$$

As evident from the curvature expressions (10), in the limit of $a \to b$

$$K_{1,2}(f)|_{f=3\pi/4,-\pi/4,} \to \mp\infty.$$

The lines in the ab plane, separating regions of positive and negative curvature $K_2(f)$ at $f = 3\pi/4$, $-\pi/4$ are solutions (a_0, b_0) to the equation

$$\Delta(a_0, b_0) = 0; \quad (12)$$

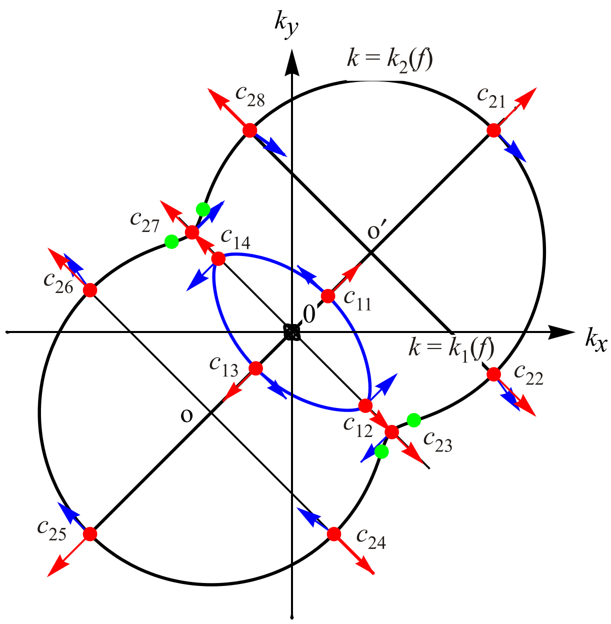

Fig. 1. Fermi contours for a combined R-D SOI. Red vectors indicate the velocity direction, blue—spin direction. Green points correspond to the FC inflection points. c_{ik}—(red) points where the velocity vector is oriented along the symmetry axis.

where

$$\Delta(a,b) = |a-b|\sqrt{(a-b)^2+1} - 4ab, \tag{13}$$

reduces to a cubic equation with known solutions.

The shaded area in Fig. 2 shows the region of (a, b) parameters $\Delta(a, b) > 0$, where the $\epsilon_2(\mathbf{k}) = \epsilon_F$FC is convex. The red curves correspond to the pair of points (a_0, b_0) satisfying Eq. (12).

The non-convex contour ($\Delta(a, b) < 0$) contains four inflection points f_i, shown as green points in Fig. 1 and positioned symmetrically with respect to the $k_x = -k_y$ line,

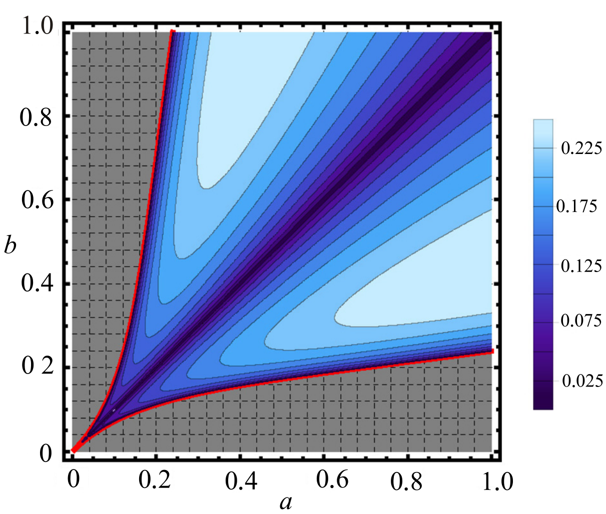

Fig. 2. The shaded area corresponds to the values of the (a, b) parameters with $\Delta(a, b) > 0$. Red curves run along the boundary values $\Delta(a, b) = 0$. Contours corresponding to constant values of the $\Delta f_{\rm in}(a,b) = $const angle, that determines the positions of the inflection points (14), are shown in the region where $\Delta(a, b) < 0$.

$$\begin{aligned} f_{1,2}(a,b) &= 3\pi/4 \mp \Delta f_{\rm in}(a,b), \\ f_{3,4}(a,b) &= -\pi/4 \pm \Delta f_{\rm in}(a,b). \end{aligned} \tag{14}$$

It can be shown that the function $\Delta f_{\rm in}(a,b)$ possesses the following properties:

$$\lim_{a\to b} \Delta f_{\rm in}(a,b) = \Delta f_{\rm in}(a_0,b_0) = 0. \tag{15}$$

To determine the f_i angles, the solution to the $K_2(f = f_i) = 0$ equation can be reduced to an algebraic equation in the fourth power of the sin(2f) function, the solution to which can be found in standard references (see for example Ref. 27). We do not present the concrete expression for $\Delta f_{\rm in}$, determining all four inflection points (14) due its cumbersome size. Figure 2 shows the $\Delta f_{\rm in} = $const contours for different values of the R-D SOI constants.

2.3. Green's function

At zero temperature, LDOS $\rho(\epsilon_F, \boldsymbol{\rho})$ and LMD $\mathbf{M}(\epsilon_F, \boldsymbol{\rho})$ can be written down using a retarded Green's function $\hat{G}^R(\epsilon_F, \boldsymbol{\rho}, \boldsymbol{\rho}')$ in the coordinate representation

$$\rho(\epsilon_F, \boldsymbol{\rho}) = -\frac{1}{\pi}{\rm Im}\,Sp\left[\hat{G}^R(\epsilon_F, \boldsymbol{\rho}, \boldsymbol{\rho})\right], \tag{16}$$

$$\mathrm{M}(\epsilon_F, \boldsymbol{\rho}) = -\frac{1}{\pi}{\rm Im\,Sp}\left[\hat{\boldsymbol{\sigma}}\hat{G}^R(\epsilon_F, \boldsymbol{\rho}, \boldsymbol{\rho})\right]. \tag{17}$$

We account for the influence of the electron scattering from the defect using the Born approximation (see for example Ref. 28) with a scattering potential (5), and express the Green's function in terms of a decomposition

$$\begin{aligned} \hat{G}^R(\epsilon_F, \boldsymbol{\rho}, \boldsymbol{\rho}') \approx{}& \hat{G}_0^R(\epsilon_F, \boldsymbol{\rho}, \boldsymbol{\rho}') \\ &+ \hat{G}_0^R(\epsilon_F, \boldsymbol{\rho}, \boldsymbol{\rho}_0)\left(\gamma\hat{\sigma}_0 + \frac{1}{2}\mathbf{J}\hat{\boldsymbol{\sigma}}\right)\hat{G}_0^R(\epsilon_F, \boldsymbol{\rho}_0, \boldsymbol{\rho}'), \end{aligned} \tag{18}$$

where $\hat{G}_0^R(\epsilon_F, \boldsymbol{\rho}, \boldsymbol{\rho}')$ is the retarded Green's function in the absence of defects, that only depends on the difference between the coordinates $\mathbf{r} = \boldsymbol{\rho} - \boldsymbol{\rho}'$, and can be written as a sum

$$\hat{G}_0^R(\mathbf{r}) = \rho_{2D}(\epsilon_F)\left[g_0(\mathbf{r})\hat{\sigma}_0 + g_x(\mathbf{r})\hat{\sigma}_x + g_y(\mathbf{r})\hat{\sigma}_y\right], \tag{19}$$

where $\rho_{2D}(\epsilon_F) = m/\pi\hbar^2$ is the density of states for an ideal, degenerate two-dimensional gas. The dimensionless scalar function $g_{0,x,y}$ can be conveniently represented as

$$g_0(\mathbf{r}) = \frac{1}{2\pi}\sum_{j=1,2}\int_0^\pi df\,\frac{\kappa_j(f)}{\kappa_F(f)}\mathrm{A}\left(\tilde{r}S_j(f,\varphi)\right), \tag{20}$$

$$\begin{aligned} g_x(\mathbf{r}) = -\frac{i}{2\pi}\sum_{j=1,2}(-1)^j\int_0^\pi df\,\frac{\kappa_j(f)}{\kappa_0(f)\kappa_F(f)}(a\sin f + b\cos f) \\ \times \mathrm{B}\left(\tilde{r}S_j(f,\varphi)\right), \end{aligned} \tag{21}$$

$$\begin{aligned} g_y(\mathbf{r}) = \frac{i}{2\pi}\sum_{j=1,2}(-1)^j\int_0^\pi df\,\frac{\kappa_j(f)}{\kappa_0(f)\kappa_F(f)}(b\sin f + a\cos f) \\ \times \mathrm{B}\left(\tilde{r}S_j(f,\varphi)\right), \end{aligned} \tag{22}$$

where the angle φ determines the direction of the dimensionless vector of the $\tilde{\mathbf{r}} = \tilde{r}(\cos\varphi,\ \sin\varphi)$, $\tilde{r} = k_F r$, coordinate, in the xy plane of the 2D electron gas,

$$S_j(f,\varphi) = \kappa_j(f)\cos(f-\varphi), \tag{23}$$

$$\mathrm{A}(x) = \cos(x)\mathrm{Ci}(|x|) + \sin(x)\mathrm{Si}(x) - \frac{i\pi}{2}\cos(x); \tag{24}$$

$$\mathrm{B}(x) = \sin(x)\mathrm{Ci}(|x|) - \cos(x)\mathrm{Si}(x) - \frac{i\pi}{2}\sin(x), \tag{25}$$

$\mathrm{Si}(x)$ and $\mathrm{Ci}(|\,x\,|)$ are the integral sine and cosine respectively. Expressions (19)–(22) are analogous to those of Ref. 29.

The $g_{0,x,y}$ components of the Green's function (19) satisfy the symmetry relations

$$g_0(-\mathbf{r}) = g_0(\mathbf{r}), \quad g_{x,y}(-\mathbf{r}) = -g_{x,y}(\mathbf{r}), \tag{26}$$

$$\begin{aligned} g_x(x,y) &= -g_y(x,y), \quad at\, x = y, \\ g_x(x,y) &= g_y(x,y), \quad at\, x = -y, \end{aligned} \tag{27}$$

allowing significant simplification of subsequent calculations.

3. LDOS oscillations

3.1. General picture of the LDOS oscillations

The anisotropic dispersion relation leads to several interesting features of the elastic scattering of a charged carrier from the defects (see for example Ref. 30). The scattering angle is determined by the direction of the velocity, which does not necessarily coincide with the direction of the wavevector. Moreover, for a nonconvex energy surface, a single scattering angle corresponds to several values of the wavevector.[30] However, if the isoenergetic surface has a flattening (where the curvature is small and the velocity barely changes), an enhanced electronic current appears in the direction of its normal.[31] Reference 32 shows that the geometry of the constant-phase lines for Friedel-type oscillations in the LDOS depends on the local FC geometry of the 2D electrons $\epsilon(\mathbf{k}) = \epsilon_F$. The amplitude of the oscillations in a particular direction $\boldsymbol{\rho}$, lying in real space and at a large distance from the defect is determined by the curvature of the FC at a point where the electron velocity, $\mathbf{v} = d\epsilon(\mathbf{k})/\hbar d\mathbf{k}$, is oriented along $\boldsymbol{\rho}$.[32] The period of the oscillation, $\Delta r = \pi/S$, depends on the projection S of the wavevector $\mathbf{k}$ onto the direction $\mathbf{v}$. The features of the electron scattering in conductors with anisotropic dispersion relations should appear in the Friedel oscillations of LDOS and LMD in the presence of a combined R-D SOI.

Using expressions (16), (18), (19), and (26) we can write down the LDOS as

$$\boldsymbol{\rho}(\epsilon_F,\mathbf{r}) = \boldsymbol{\rho}_{2D}(\epsilon_F)\left[1 + \Delta\boldsymbol{\rho}(\epsilon_F,\mathbf{r})\right], \tag{28}$$

$$\begin{aligned} \Delta\boldsymbol{\rho}(r) = -\frac{2}{\pi}\gamma\boldsymbol{\rho}_{2D}\{&\mathrm{Im}g_0(\mathbf{r})\mathrm{Re}g_0(\mathbf{r}) - \mathrm{Im}g_x(\mathbf{r})\mathrm{Re}g_x(\mathbf{r}) \\ &- \mathrm{Im}g_y(\mathbf{r})\mathrm{Re}g_y(\mathbf{r})\}. \end{aligned} \tag{29}$$

As in the case of either Rashba or Dresselhaus SOI, the magnetic part of the scattering potential (that is proportional to $\mathbf{J}$) of the combined SOI does not contribute to the LDOS.

Figure 3(a) shows a characteristic shape of the $\Delta\boldsymbol{\rho}(\tilde{x},\tilde{y})$ spatial distribution with parameter values corresponding to $\Delta(a,b) < 0$ (12), which leads to the outer FC, $k = k_2(f,\ \epsilon_F)$ having four inflection points (14) (green points on the outside contour of Fig. 1). The amplitude of the Friedel oscillations of the LDOS is maximum for directions coinciding with that of the velocity $\mathbf{v}_2(f_i) = d\epsilon_2/\hbar d\mathbf{k}$ at the zero-curvature points f_i (14).

The "fan" of directions that contain additional oscillation harmonics is bounded, at the inflection points f_i (14) of the outer FC curve, by the angles of the charged carrier velocity vector. Red lines in Fig. 3(a) show directions in real space that bound the $\Delta\theta$ angle. The tangent of the $\theta_i = \theta(f_i)$ angle can be determined from the ratio of the velocity components: $\mathrm{tg}(\theta_i) = \nu_{x2}(f_i)/\nu_{y2}(f_i)$. We do not present the concrete form of the $\theta_i = \theta(a,b)$ functions due to their overly cumbersome size. It follows from expressions (15), that the $\Delta\theta$ "fan" collapses and the amplitude of the LDOS oscillations is maximum for the $\tilde{x} = -\tilde{y}$ direction [see Fig. 3(b)] at the boundary values of the SOI constants $(a_0,\ b_0)$ (12), where the convexity of the outer FC disappears, and when $a = b$. The amplitude of the LDOS oscillations at the "fan" boundaries is determined by pairs of points: the inflection point and the point of zero curvature.

To analyze the dependence of Friedel oscillations of the LDOS on the SOI constants, we obtain asymptotic expressions for the general formula (29) at large distances from the defect. When $\kappa_{1,2}r \gg 1$ (see Ref. 32) the main contribution to the LDOS oscillations $\rho(\epsilon_F,\ \mathbf{r})$ comes from the FC points

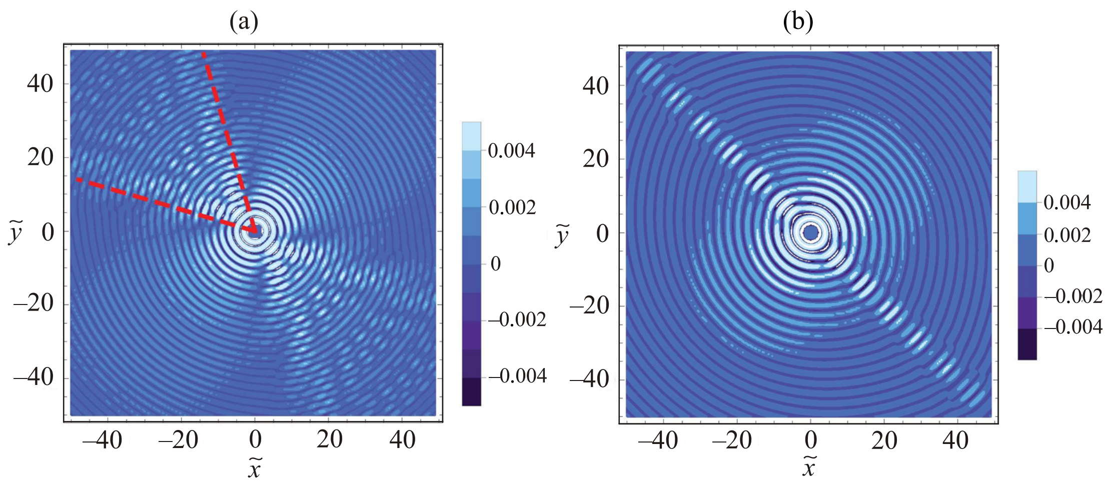

Fig. 3. Local density of states $\Delta\boldsymbol{\rho}(\tilde{x},\tilde{y})$ with (a) $a = 0.7$, $b = 0.5$; (b) $a = 0.7$, $b = 0.19976$.

where the velocities of the electron impinging and backscattering from the defect are oriented along **r**. These asymptotes assume the simplest form for directions coinciding with the $\tilde{x}=\tilde{y}$ and $\tilde{x}=-\tilde{y}$ symmetry axes. In this case, the constant-phase points of the fast-oscillating functions (23) in the integrals (20)–(22) coincide with the FC points (red c_{ik} points in Fig. 1) where the electron velocities (shown as red arrows) are oriented along the symmetry axes. For the $x=-y$ direction, along with the contribution of the points where $\mathbf{v}_{1,2}||\mathbf{k}$ (points c_{11}, c_{31}, c_{23}, c_{27} in Fig. 1), the LDOS oscillations contain harmonics, caused by the presence of additional points on the outer FC (points c_{22}, c_{24}, c_{26}, c_{28} in Fig. 1). These points do not lie on the contour symmetry axis, but their corresponding velocity vector $\mathbf{v}_2(f)$ is parallel to the $k_x=-k_y$ direction.

3.2. LDOS oscillations along the $x=\pm y$ symmetry axes

The $\mathbf{v}_{1,2}||\mathbf{k}$ velocity vectors along the $x=y$ direction correspond to the FC points that lie along the $k_x=k_y$ symmetry axis (points c_{14}, c_{34}, c_{21}, c_{25} in Fig. 1). Substituting the asymptotic expressions (A.7) for the $g_i(\mathbf{r})$ Green's function components into Eq. (29) yields the following expression for the additional dimensionless oscillating contribution $\Delta\rho(\epsilon_F, \mathbf{r})$ to the LDOS:

$$\Delta\rho(r) \simeq -\gamma\rho_{2D}\frac{\Phi_1^0\Phi_2^0}{\tilde{r}\sqrt{|S_1''S_2''|}}\cos\left[\tilde{r}(S_1+S_2)\right], \tag{30}$$

where the $S_{1,2}(\varphi,f)$ (23) functions are taken at the values of the $x=y$ line (i.e., when $\varphi=\pi/4$) and at the stationary phase points $f_1^{\mathrm{st}}=\pi/4$

$$S_{1,2}=\sqrt{(a+b)^2+1}\mp(a+b). \tag{31}$$

These values are determined by the magnitudes of the wavevectors oriented towards the c_{11}, c_{13} and the c_{21}, c_{25} FC points (see Fig. 1). The Appendix contains the coefficients $\Phi_{1,2}$ (A.8) and the second derivatives $S''_{1,2}$ (A.9) which are related to the curvature of the contours $K_{1,2}$ [see Eq. (A.4) in the Appendix] with $\operatorname{sgn}S''_{1,2}(f)=-\operatorname{sgn}K_{1,2}(f)$.

Presence of a single harmonic in the expression (30), that is dependent on the sum of the wavevectors belonging to different contours, can be explained by the fact that the pairs of points c_{11}, c_{13} and c_{21}, c_{25} (see Fig. 1) belonging to the same FC, correspond to opposite directions of the spin. The orthogonality properties of the spin part of the wavefunction for opposing wavevector directions (4) lead to the lack of corresponding contributions to the LDOS.

For the $x=-y$ direction, when $\Delta(a,b)>0$ (13), i.e., in the absence of concave FC regions, the asymptotic form of the LDOS oscillations is determined by the stationary phase point $f_1^{\mathrm{st}}=3\pi/4$ and can also be written in the form of (30). The $S_{1,2}$, $K_{1,2}$ functions for the $x=-y$ direction (i.e., when $\varphi=3\pi/4$) have the form:

$$S_{1,2}=\sqrt{(a-b)^2+1}\mp|a-b|. \tag{32}$$

The values of the $\Phi^0_{1,2}$ and $S''_{1,2}$ functions are determined by formulas (A.10) and (A.11) of the Appendix.

In the presence of concave regions on the outer FC, $\Delta(a,b)<0$ (13), the LDOS oscillations contain harmonics due to the additional stationary phase points c_{22}, c_{24}, c_{26}, c_{28} (Fig. 1). The values of the angles $f^{st}_{3,4}=3\pi/4\pm\Delta f_{st}$ (A.5), that determine the wavevector direction oriented towards these points can be found in the Appendix. Utilizing the asymptotic expression for the components of the Green's function $g_i(\mathbf{r})$ (A.12), we arrive at the following expression for the oscillatory part of the LDOS:

$$\begin{aligned}\Delta\rho(r) \approx \frac{\gamma\rho_{2D}}{\tilde{r}}\Bigg\{&\frac{\Phi_1^0\Phi_2^0}{\sqrt{|S_1''S_2''|}}\sin\left(\tilde{r}(S_1+S_2)\right)\\ &+\frac{\Phi_2^0\left(\sqrt{2}\Phi_{\mathrm{add}}-\Phi_{\mathrm{sum}}\right)}{\sqrt{2}\sqrt{|S_2''S_3''|}}\sin\left(\tilde{r}(S_2+S_3)\right)\\ &-\frac{\Phi_1^0\left(\sqrt{2}\Phi_{\mathrm{add}}+\Phi_{\mathrm{sum}}\right)}{\sqrt{2}\sqrt{|S_1''S_3''|}}\cos\left(\tilde{r}(S_1+S_3)\right)\\ &+\frac{\Phi^2_{\mathrm{sum}}-2\Phi^2_{\mathrm{add}}}{2|S_3''|}\cos\left(2\tilde{r}S_3\right)\Bigg\},\end{aligned} \tag{33}$$

where

$$S_3=S_2\left(f^{\mathrm{st}}_{3,4},\frac{3\pi}{4}\right)=\frac{(a+b)\sqrt{(a+b)^2+1}}{2\sqrt{ab}}, \tag{34}$$

definitions of $\Phi^0_{1,2}$ (A.10), Φ_{add} (A.14), Φ_{sum} (A.13), $S''_{1,2}$ (A.11), S''_3 (A.15) at the corresponding points of stationary phase are presented in the Appendix. The following inequality becomes apparent from examining Fig. 1:

$$\begin{aligned}S_1+S_2&=c_{23}0+0c_{14}<S_1+S_3=c_{12}0+oc_{26}<S_2+S_3\\ &=c_{23}0+oc_{26}<2S_3=c_{24}c_{26},\end{aligned} \tag{35}$$

and enables identification of every harmonic during Fourier analysis of the experimental data. As in the expression (30), formula (33) lacks contributions from pairs of FC points positioned symmetrically relative to the origin of the coordinates for which the spins are necessarily antiparallel. Presence of the additional periods of oscillations is related to the nonzero probability of backscattering from $c_{22}(c_{28})$, $c_{24}(c_{26})$ points to $c_{28}(c_{22})$, $c_{26}(c_{24})$, $c_{27}(c_{23})$ points of the same FC and to the $c_{14}(c_{12})$ points from the inner contour, where the spins are not parallel to the electron spins prior to scattering.

Each harmonic of the LDOS $\Delta\rho(\tilde{r})$ (30), (33) is due to a pair of points on the FC, that are related to the S_i+S_j sums, that determine the LDOS oscillation periods in the coordinate space

$$\Delta r_{ij}(f)=\frac{2\pi}{k_F(S_i+S_j)}, \tag{36}$$

containing information about the SOI constants.

4. LMD oscillations

Using the $\mathbf{M}(\mathbf{r})$ expression (17) to describe the LDOS and expanding the Green's function in terms of the Pauli matrices (19), we can write the vector components of $\mathbf{M}(\mathbf{r})$ in the following form:

$$M_x = -\frac{2}{\pi}\rho_{2D}^2 \mathrm{Im}\Big\{J_x\Big[g_0^2(\mathbf{r}) - g_x^2(\mathbf{r}) + g_y^2(\mathbf{r})\Big] - 2J_y g_x(\mathbf{r})g_y(\mathbf{r}) + 2iJ_z g_0(\mathbf{r})g_y(\mathbf{r})\Big\}, \tag{37}$$

$$M_y = -\frac{2}{\pi}\rho_{2D}^2 \mathrm{Im}\Big\{J_y\Big[g_0^2(\mathbf{r}) + g_x^2(\mathbf{r}) - g_y^2(\mathbf{r})\Big] - 2J_x g_x(\mathbf{r})g_y(\mathbf{r}) - 2iJ_z g_0(\mathbf{r})g_x(\mathbf{r})\Big\}, \tag{38}$$

$$M_z = -\frac{2}{\pi}\rho_{2D}^2 \mathrm{Im}\Big\{J_z\Big[g_0^2(\mathbf{r}) + g_x^2(\mathbf{r}) + g_y^2(\mathbf{r})\Big] - 2iJ_x g_0(\mathbf{r})g_y(\mathbf{r}) + 2iJ_y g_0(\mathbf{r})g_x(\mathbf{r})\Big\}. \tag{39}$$

It is clear the LMD only depends on the magnetic part of the impurity potential (5).

In contrast to the LDOS, the contributions to the LMD comes from scattering processes accompanied by a spin-flip. Friedel oscillations of the LMD develop harmonics due to the interference of contributions, characterized by opposite spin directions (c_{11}, c_{13} and c_{21}, c_{25} pairs of points in Fig. 1).

Many features of the LMD oscillations can be understood from the following considerations. The squared moduli of the matrix elements belonging to backscattering between states belonging to the same or different FC are calculated using the function (3) and have the form

$$|\hat{\varphi}_{1,2}^{\dagger}(\theta)\mathbf{J}\boldsymbol{\sigma}\hat{\varphi}_{1,2}(\theta+\pi)|^2 = |J_z|^2 + |J_x\cos\theta + J_y\sin\theta|^2 = |J_z|^2 + \left|\left[\mathbf{J}\times \mathrm{s}_{1,2}(\theta)\right]_z\right|^2, \tag{40}$$

$$|\hat{\varphi}_{1,2}^{\dagger}(\theta)\mathbf{J}\boldsymbol{\sigma}\hat{\varphi}_{2,1}(\theta+\pi)|^2 = |J_y\cos\theta - J_x\sin\theta|^2 = |\mathbf{J}\mathbf{s}_{1,2}(\theta)|^2. \tag{41}$$

If the $\mathbf{J}$ vector is perpendicular to the spin direction $\mathbf{s}_{1,2}$, backscattering occurs into a state on the same FC with an opposite spin. However, if the $\mathbf{J}$ and $\mathbf{s}_{1,2}$ vectors are collinear, the electron spin is conserved, whereas the state after scattering belongs to a different FC as in the case of a nonmagnetic defect.

4.1. The effective magnetic moment of the defect is perpendicular to the plane of a 2D conductor

In this case, the effective magnetic moment of the defect $\mathbf{J} = (0,0,J)$ is always perpendicular to the spin of the 2D electron, lying in the plane. Due to the features of the matrix elements (40), (41), contributions to the LMD oscillations come from backscattering with a complete spin flip and a transition to a state on the same FC. In the case of backscattering, transitions between different contours are only possible for states on the nonconvex FC, in the points where the velocity is oriented at an angle to the wavevector. Figure 4 shows the characteristic shape of the LMD Friedel oscillations.

In contrast to the LDOS, the large amplitude of the LMD oscillations in Fig. 4, for directions determined by the inflection points, is due to backscattering processes with a spin flip accompanied by a transition between two states corresponding to the zero curvature of the outer FC and the opposite direction of the velocity and the wavevector.

We introduce an asymptotic expression for the oscillations in the $x = \pm y$ LDOS vector directions when $\tilde{r} \gg 1$, by expressing them as a sum of two terms,

$$M_i(\tilde{r}) = M_i^{(1)}(\tilde{r}) + \chi M_i^{(2)}(\tilde{r}), \tag{42}$$

where $M_i^{(1)}(\tilde{r})$ is the contribution of the stationary phase points $f_{1,2}^{\mathrm{st}} = \pi/4, 3\pi/4$, lying on the symmetry axes and $M_i^{(2)}(\tilde{r})$ is the contribution of the additional points $f_{3,4}^{\mathrm{st}}$ (A.5) into the $x = -\,y$ direction, that appear on the outer contour in the presence of a concave region which only exists when $\Delta(a,b) < 0$ (13),

$$\chi = \Theta(-\Delta(a,b))\Theta(-xy), \tag{43}$$

$\Theta(x)$ is the Heaviside function. In the formula (42)

$$M_z^{(1)} \approx -\frac{\rho_{2D}^2}{2\tilde{r}}J\left[\frac{\left(\Phi_1^0\right)^2}{|S_1''|}\cos(2\tilde{r}S_1) + (1-2\chi)\frac{\left(\Phi_2^0\right)^2}{|S_2''|}\cos(2\tilde{r}S_2)\right], \tag{44}$$

$$M_z^{(2)} \approx -\frac{\rho_{2D}^2 J}{2\tilde{r}}\left[\frac{\left(\Phi_{\mathrm{sum}}^2 + 2\Phi_{\mathrm{add}}^2\right)}{|S_3''|}\cos(2\tilde{r}S_3) - \sqrt{2}\frac{\Phi_1^0\left(\Phi_{\mathrm{sum}} - \sqrt{2}\Phi_{\mathrm{add}}\right)}{\sqrt{|S_1''S_3''|}}\cos(\tilde{r}(S_1+S_3)) - \sqrt{2}\frac{\Phi_2^0\left(\Phi_{\mathrm{sum}} - \sqrt{2}\Phi_{\mathrm{add}}\right)}{\sqrt{|S_2''S_3''|}}\sin(\tilde{r}(S_2+S_3))\right], \tag{45}$$

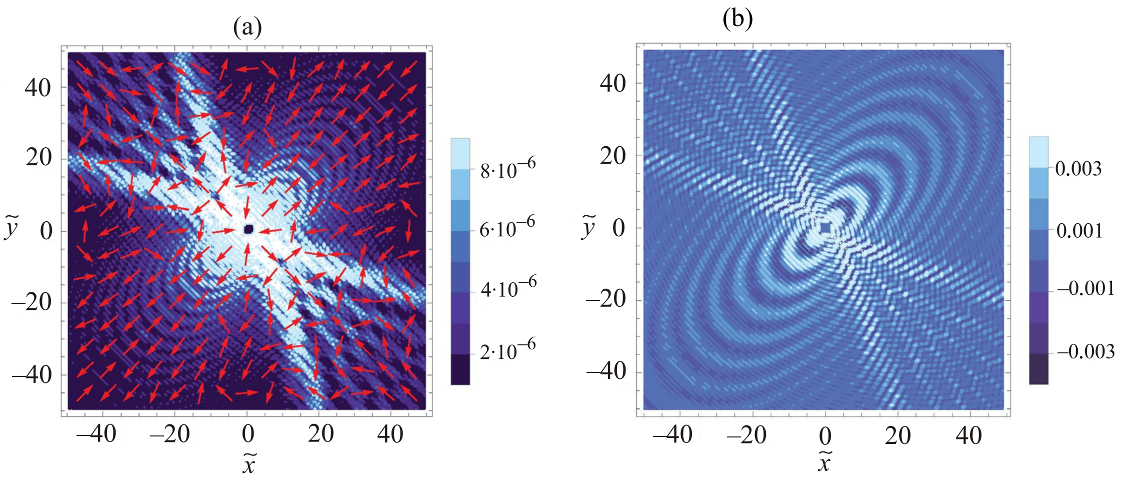

Fig. 4. Magnetization in the $M_{x,y}(\tilde{x},\tilde{y})$ conductor plane (direction and the square projection of the vector onto the plane) (a) $M_z(\tilde{x},\tilde{y})$ component (b) $a = 0.7$, $b = 0.5$ due to an impurity with an effective magnetic moment, $\mathbf{J} = J(0,0,1)$ and normalized to $M_0 = m^2 J/\hbar^4$.

where $S_{1,2,3}$ correspond to expressions (31) and (34) for $y=-x>0$ directions, and the expressions for $\Phi^0_{1,2}$ (A.10), $S''_{1,2}$ (A.11), $\Phi_{\rm add}$ (A.14), $\Phi_{\rm sum}$ (A.13) and $S''_{1,3}$ (A.15) are defined in the Appendix. For the $y=x>0$ direction, the $S_{1,2}$ functions are defined by the expression (31), while the expressions for the $\Phi_{1,2}$ coefficients and the $S''_{1,2}$ second derivatives (A.9) are listed in the Appendix.

It is easy to notice, that aside from the frequencies present in the LDOS oscillation spectrum (33), expression (45) also contains harmonics with frequencies defined by chords [(c_{12}, c_{14}) and (c_{23}, c_{27}) point in Fig. 1] of the small and the large FC, respectively. Due to the symmetry of the FC, each one of these harmonics is defined by the FCs characteristics at only a single point (c_{12}, c_{14}, c_{23}, c_{27}) simplifying the problem of reconstructing the SOI constants.

For the $x=\pm y$ direction, the projection of the LMD vector onto the conductor plane will be parallel to **r**

$$M_x = \pm M_y = M^{(1)}(\tilde{r}) + \chi M^{(2)}(\tilde{r}). \tag{46}$$

For the $x=y$ direction, in the case of $\tilde{r}\gg 1$, the LMD oscillations in the conductor plane will be determined by the expression

$$M_{x,y} = M^{(1)} \simeq \frac{\rho_2^2 DJ}{2\sqrt{2\tilde{r}}}\left[\frac{(\Phi_2^0)^2}{|S_2''|}\sin(2\tilde{r}S_2) - \frac{(\Phi_1^0)^2}{|S_1''|}\sin(2\tilde{r}S_1)\right]. \tag{47}$$

Notably, the appearance of in-plane components is a consequence of the SOI, since in its absence the LMD vector would be parallel to the **J** vector.

For the $x=-y$ direction, the $M_x=-M_y$ LMD components (46) can be represented by the following functions:

$$M^{(1)} \simeq \frac{\rho_2^2 DJ_0}{2\sqrt{2\tilde{r}}}\,\mathrm{sgn}(a-b) \times\left[\frac{(\Phi_1^0)^2}{|S_1''|}\sin(2\tilde{r}S_1) - \frac{(\Phi_2^0)^2}{|S_2''|}\sin(2\tilde{r}S_2)\mathrm{sgn}\Delta(a,b)\right], \tag{48}$$

$$M^{(2)} \simeq -\rho_{2D}^2 J_0 \mathrm{sgn}(a-b)\left[\frac{\Phi_{\rm add}\Phi_{\rm sum}}{\tilde{r}|S_3''|}\sin(2\tilde{r}S_3) + \frac{\Phi_1^0(\Phi_{\rm sum}-\sqrt{2}\Phi_{\rm add})}{2\tilde{r}\sqrt{|S_1''S_3''|}}\sin(\tilde{r}S_1+S_3)) + \frac{\Phi_2^0(\Phi_{\rm sum}+\sqrt{2}\Phi_{\rm add})}{2\tilde{r}\sqrt{|S_2''S_3''|}}\cos(\tilde{r}S_2+S_3))\right]. \tag{49}$$

Expression (49) changes its sign upon rearrangement of the a and b constants. In this way, investigation of the LMD allows avoiding ambiguity in determining the SOI constants.

4.2. Effective magnetic moment of an impurity lies in the plane of a 2D conductor

Figure 5 shows the characteristic shape of the LMD oscillations when the **J** vector is oriented along the $x=y$ line ($J_x=J_y$ and $J_z=0$).

Based on the properties of the backscattering matrix elements (40), (41), the formulas for the asymptotes of the M_i components contain terms of three types

$$M_i(\tilde{r}) = M_i^{(||)}(\tilde{r}) + M_i^{(\perp)}(\tilde{r}) + \chi M_i^{(2)}(\tilde{r}), \tag{50}$$

where $M_i^{(||)}(\tilde{r})$ is the scattering contribution with a conserved spin and a transition between contours (goes to zero when $\mathbf{J}||\mathrm{s}_{1,2}(f^{\rm st}_{1,2})$), $M_i^{(\perp)}(\tilde{r})$ is the scattering contribution with a spin flip without a transition between contours (goes to zero when $\mathbf{J}\perp\mathrm{s}_{1,2}(f^{\rm st}_{1,2})$), $M_i^{(2)}(\tilde{r})$ is the contribution from the $f^{\rm st}_{3,4}$ (A.5) additional points on the nonconvex contour and the χ function is defined in (43).

To illustrate this point, we introduce the asymptotic expressions for the LMD vector components in the $x=\pm y$ directions with $\mathbf{J}=J/\sqrt{2}(1,1,0)$. Based on the M_i component formulas (37)–(39), and g_i function symmetry properties (27), $M_x=M_y$, i.e., the projection of the **M** vector onto the plane is always oriented along **J**, while the $M_z\equiv 0$ component is oriented along $x=-y$.

When $x=y$, $\mathbf{J}\perp\mathrm{s}_{1,2}(\theta(\pi/4))$, due to the properties of the matrix elements (40), (41), the first ($M^{||}(\tilde{r})=0$) and the third ($\gamma=0$) terms of the general expression for M_i are absent. The M_x and M_y components of the LDOS vector are equal to

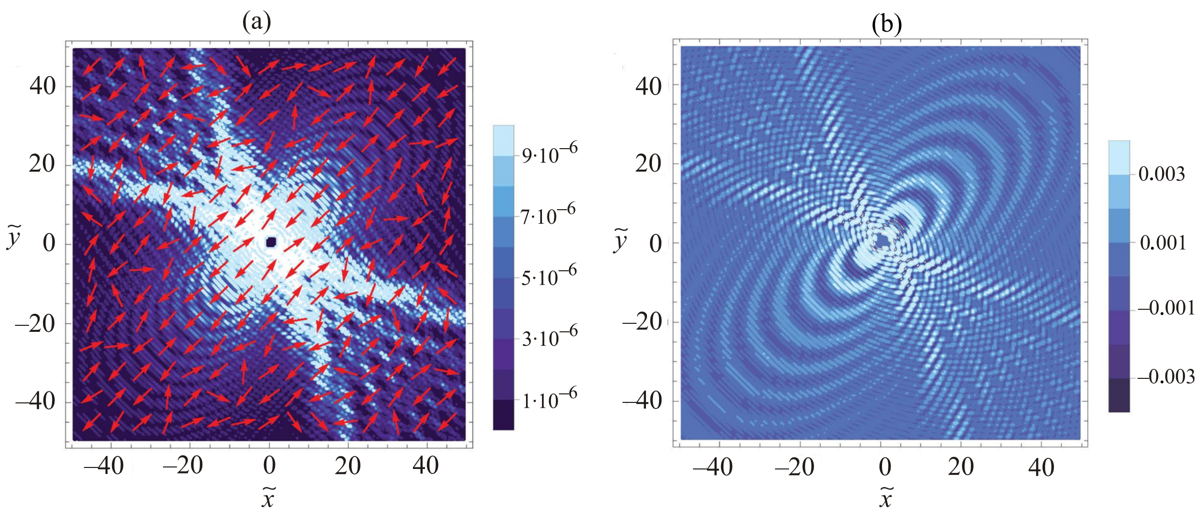

Fig. 5. LMD distribution $(M_x^2+M_y^2)/M_0$ with $a=0.7$, $b=0.5$; $\mathbf{J}=J/\sqrt{2}(1,1,0)$; $M_0=m^2J/\hbar^4$. (a) Arrows indicate the in-plane direction of the **M** vector. (b) M_z component for the same values of a,b and the direction of **J**.

$$M_{x,y}^{(\perp)}(\tilde{r}) \simeq \frac{\rho_{2D}^2 J_0}{2\sqrt{2\tilde{r}}}\left[\frac{(\Phi_1^0)^2}{|S_1''|}\cos(2\tilde{r}S_1) - \frac{(\Phi_2^0)^2}{|S_2''|}\cos(2\tilde{r}S_2)\right], \tag{51}$$

while the component perpendicular to the plane has the form

$$M_z \simeq \frac{\rho_{2D}^2 J}{2\tilde{r}}\left[\frac{(\Phi_1^0)^2}{|S_1''|}\sin(2\tilde{r}S_1) - \frac{(\Phi_2^0)^2}{|S_2''|}\sin(2\tilde{r}S_2)\right]. \tag{52}$$

For the $x = -y$, $\mathbf{J} \,||\, s_{1,2}(\theta(3\pi/4))$ direction, the $M_{x,y}^{(\perp)}(\tilde{r}) = 0$ contribution and the $M_x = M_y$ components of the magnetization contain the terms

$$M^{(||)}(\tilde{r}) \simeq -\rho_{2D}^2 J_0 \frac{\Phi_1^0\Phi_2^0}{\sqrt{2\tilde{r}}\sqrt{|S_1''S_2''|}}\cos\left(\tilde{r}(S_1+S_2) + \frac{\pi}{2}\chi\right), \tag{53}$$

$$\begin{aligned} M_{x,y}^{(2)} \simeq \frac{\rho_{2D}^2 J_0}{2\tilde{r}}\Bigg[&\frac{\Phi_{\text{sum}}^2 - 2\Phi_{\text{add}}^2}{\sqrt{2|S_3''|}}\cos[2\tilde{r}S_3] \\ &- \frac{\Phi_1^0(\Phi_{\text{sum}} + \sqrt{2}\Phi_{\text{add}})}{\sqrt{|S_1''S_3''|}}\cos(\tilde{r}(S_1+S_3)) \\ &- \frac{\Phi_2^0(\Phi_{\text{sum}} + \sqrt{2}\Phi_{\text{add}})}{\sqrt{|S_2''S_3''|}}\sin(\tilde{r}(S_1+S_3))\Bigg]. \end{aligned} \tag{54}$$

Formulas (51) and (52) show that in the direction of the defect magnetic moment $\mathbf{J}$, along the $x = y$ symmetry axis, the LDOS oscillations in the $\mathbf{J}$ direction are only determined by the backscattering processes between points of the same FC, while for the $x = -y$ direction that is perpendicular to $\mathbf{J}$, only one harmonic with a $\Delta r_{33} = \pi/S_3$ period is due to such scattering.

5. Conclusions

Using Green's functions (19)–(22) for a two-dimensional gas with a combined Rashba-Dresselhaus SOI (1) yields the general expressions for the local density of states (28) and the local magnetization density (37)–(39) in the vicinity of a point defect. Scattering of electrons by the defect is accounted for by the Born approximation. We obtain asymptotic expressions for the LDOS (30), (33) and the LMD (45) for directions coinciding with the symmetry axes of the Fermi-contours and find them to be accurate for defect distances that are much larger than the de Broglie wavelength of the electron.

The LDOS oscillations (30) along the $x = y$ symmetry axis, with a period depending on the sum of the radii S_1+S_2, of two FCs, are caused by the backscattering of electrons between FCs with a conserved spin. For a nonconvex FC, the LDOS oscillations along the $x = -y$ symmetry axis contain four harmonics (33) (as opposed to two, as asserted in Ref. 24) Aside from harmonics that depend of the S_1+S_2 sum of the FC radii, three additional harmonics are present for this direction and are due to the presence of four f_i^{st} (A.5) contour points, where the velocity vector $\mathrm{v}_2(\mathbf{k}(f_i^{\text{st}}))$ is oriented along the $k_x = -k_y$ symmetry axis, and the $\mathbf{k}(f_i^{\text{st}})$ wavevector is at an angle Δf_{st} (A.5) relative to it. We note, that backscattering of electrons from the $\mathbf{k}(f_i^{\text{st}})$ points is possible for any state with $\mathbf{v}_2(\mathbf{k}') = -\mathbf{v}_2(\mathbf{k})$ except when $\mathbf{k}' = \mathbf{k}$. These conditions determine the nonzero amplitude of the harmonics with $S_3 + Sj$ ($j = 1,2,3$) periods, where $2k_F S_3$ is the length parallel to the $k_x = -k_y$ FC chord direction connecting the f_i^{st} points.

Formulas (31) and (32) show that the ratio $\Delta r_{ij}/\Delta r_{mn}$ of the periods of two LDOS oscillation harmonics depends solely on the dimensionless SOI constants a, b and does not contain any other terms characterizing the electronic subsystem. It is possible to find a and b using two ratios of any periods. After finding the SOI constants, we can determine the valuable $k_F = \sqrt{2m\epsilon_F}/\hbar$ parameter from one of the periods.

Determination of the SOI constants from the LDOS oscillations is ambiguous. It is easy to notice that the picture of the LDOS oscillations is insensitive to rearrangement of the a and b constants or to the inversion of their sign. Investigation of the LMD Friedel oscillations can aid in unambiguous identification of the SOI constants. For example, according to the results in (46)–(49) in the case when the magnetic moment of the defect is perpendicular to the xy plane of the 2D electron gas, the phase of the $M_{\text{x,y}}$ components of the LMD oscillations for $a > b$ and $a < b$ differs by π.

One of the authors (Yu.A.) expresses deep gratitude to A. N. Omel'yanchuk for many years of productive collaboration and numerous discussions of physics of normal and superconducting systems.

APPENDIX: ASYMPTOTIC GREEN'S FUNCTIONS

Let's consider the asymptotic behavior of the $g_0, x, y(\tilde{\mathbf{r}})$ (20)–(22) functions for large values of the dimensionless coordinate, $\tilde{r} \gg 1$. Using the approximate expressions for the $\mathrm{A}(x)$ (24) and $\mathrm{B}(x)$ (25) functions for large values of the argument, $|x| \gg 1$

$$A(x) \simeq i\mathrm{B}(x)\mathrm{sgn}(x) \simeq -\frac{i\pi}{2}\mathrm{e}^{i|x|}, \tag{A.1}$$

we write the integrals (21) and (22) in the form

$$g_i(\tilde{\mathbf{r}}) \simeq \frac{i}{4}\sum_{j=1,2} c_j^i \int_0^{\pi} df\,\Phi_j^i(f)\exp\left(i\tilde{r}S_j(f,\varphi)\right), \tag{A.2}$$

where $c_j^0 = 0$, $c_j^x = (-1)^j$ and $c_j^y = (-1)^{j+1}$. The exact form of the $\Phi_j^i(f)$ functions, and the sign before the expression are clear from formulas (20)–(22). $\Phi_j^i(f)$ and $S_j(f,\varphi)$ functions are continuous and bounded for all values of the argument f. Calculation of the integrals with respect to f is possible by using the stationary phase method.[41] The points of stationary phase, $f = f^{\text{st}}(\varphi)$, can be found from

$$\left.\frac{\partial S_j(f,\varphi)}{\partial f}\right|_{f=f^{\text{st}}} = 0. \tag{A.3}$$

The second derivative, $\partial^2 S_j/\partial f^2$ is simply related to the contour curvature, K_j

$$S_j''(f) = -k_F K_j(f)\left(\kappa_j'(f)^2 + \kappa_j(f)^2\right). \tag{A.4}$$

We assume that $\partial^2 S_2/\partial f^2 \neq 0$. The $2k_F S_j(f^{\text{st}})$ term corresponds to the FC chord length oriented perpendicular to the curve normal at the $f = f^{\text{st}}$ point.

Keeping in mind the symmetry of the problem, we consider the regions with $0 \le f$, $\varphi \le \pi$, the upper half-plane in the coordinate space and the wavevector space. For the $x = y$, $\varphi = \pi/4$ direction, each contour contains a single stationary phase point $f_1^{\text{st}}(\varphi = \pi/4) = \pi/4$ (c_{11}, c_{21} points in Fig. 4).

In the $x = -y$, $\varphi = 3\pi/4$ direction, along with the $f_2^{st}(\varphi = 3\pi/4) = 3\pi/4$ points (c_{14}, c_{27} points in Fig. 4), in presence of regions with a negative curvature $\Delta(a,b) < 0$ (13) there exist two additional stationary points that do not lie on the symmetry axis (c_{26},c_{28} points in Fig. 4)

$$f_{3,4}^{st}(\varphi = 3\pi/4) = \frac{3\pi}{4} \pm \Delta f_{st}; \quad \Delta f_{st} = \frac{1}{2}\arcsin\left(\frac{(a^2-b^2)^2 + (a^2-b^2)}{2ab\left(2(a+b)^2+1\right)}\right). \tag{A.5}$$

Using expression (A.1), the asymptotes of the Green's function components, $g_i(\tilde{\mathbf{r}})$ (20)–(22), can be written down in general form:

$$g_i(\tilde{\mathbf{r}}) \simeq \frac{i}{4}\sum_{j=1,2}\sum_s c_j^i \sqrt{\frac{2\pi}{S_j''(f_s^{st})}}\Phi_j^i(f_s^{st})\exp\left(i\tilde{r}S_j(\varphi, f_s^{st}) + \frac{i\pi}{4}\mathrm{sgn}S_j''(f_s^{st})\right), \quad \tilde{r} \to \infty. \tag{A.6}$$

Indices i and j enumerate the $g_i(\tilde{\mathbf{r}})$ components and the contours, respectively. Summing over s is performed over the stationary phase points on the $j = 2$ contour.

1. Fermi contours do not contain concave regions $\Delta(a,b) > 0$

At large values of $\tilde{r}$, the components of the Green's function, $g_i(\tilde{\mathbf{r}})$ (20)–(22) have the form

$$g_i \simeq \frac{i}{4}\sum_{j=1,2} c_j^i \sqrt{\frac{2\pi}{|S_j''|\tilde{\mathbf{r}}}}\Phi_j^i \exp\left(iS_j\tilde{r} - \frac{i\pi}{4}\right)\bigg|_{f=f_k^{st}}. \tag{A.7}$$

For the $x = y$, $\varphi = \pi/4$ direction at the stationary phase point, $f_1^{st}(\varphi = \pi/4) = \pi/4$

$$\Phi_{1,2}^0 = 1 \mp \frac{(a+b)}{\sqrt{1+(a+b)^2}}, \quad \Phi_{1,2}^x = -\Phi_{1,2}^y = \frac{1}{\sqrt{2}}\Phi_{1,2}^0, \tag{A.8}$$

$$S_{1,2}''\left(\frac{\pi}{4},\frac{\pi}{4}\right) = -\frac{\left((a+b)\sqrt{(a+b)^2+1} \mp 4ab\right)\left(\sqrt{(a+b)^2+1} \mp (a+b)\right)}{(a+b)\sqrt{(a+b)^2+1}}, \tag{A.9}$$

the $S_{1,2}(\frac{\pi}{4},\frac{\pi}{4})$ functions are introduced in (31).

For the $x = -y$, $\varphi = 3\pi/4$ direction, at the stationary phase point, $f_2^{st}(\varphi = 3\pi/4) = 3\pi/4$

$$\Phi_{1,2}^0 = 1 \mp \frac{|a-b|}{\sqrt{1+(a-b)^2}}, \quad \Phi_{1,2}^x = -\Phi_{1,2}^y = \frac{\mathrm{sgn}(a-b)}{\sqrt{2}}\Phi_{1,2}^0. \tag{A.10}$$

$$S_{1,2}''\left(\frac{3\pi}{4},\frac{3\pi}{4}\right) = -\frac{\left(|a-b|\sqrt{(a-b)^2+1} \pm 4ab\right)\left(\sqrt{(a-b)^2+1} \mp |a-b|\right)}{|a-b|\sqrt{(a-b)^2+1}}. \tag{A.11}$$

2. The outer FC contour contains convex regions $\Delta(a,b) < 0$

For the $x = -y$, $\varphi = 3\pi/4$ direction, aside from the $f_2^{st}(\varphi = 3\pi/4) = 3\pi/4$ points, there exist two additional stationary phase points $f_{3,4}^{st}(\varphi = 3\pi/4)$ (A.5). In this case, the asymptote of the $g_i(\tilde{\mathbf{r}})$ functions (20)–(22) contains four contributions:

$$\begin{aligned} g_i \simeq{}& \frac{i}{4}c_1^i\sqrt{\frac{2\pi}{|S_1''|\tilde{r}}}\Phi_1^i \exp\left(iS_1\tilde{r} - \frac{i\pi}{4}\right)\bigg|_{f=3\pi/4} + \frac{i}{4}c_2^i \\ &\times\left\{\sqrt{\frac{2\pi}{|S_2''|\tilde{r}}}\Phi_2^i \exp\left(iS_2\tilde{r} - \frac{i\pi}{4}\right)\bigg|_{f=3\pi/4} + \sqrt{\frac{2\pi}{|S_2''|\tilde{r}}}\Phi_2^i \exp\left(iS_2\tilde{r} - \frac{i\pi}{4}\right)\bigg|_{f=f_3^{st}} + \sqrt{\frac{2\pi}{|S_2''|\tilde{r}}}\Phi_2^i \exp\left(iS_2\tilde{r} - \frac{i\pi}{4}\right)\bigg|_{f=f_4^{st}}\right\}, \end{aligned} \tag{A.12}$$

where $\Phi_{1,2}^j, S_{1,2}, S_{1,2}''$ and $f = f_2^{st} = 3\pi/4$ are defined by Eqs. (A.10) and (A.11), the expression for $S_3 = S_2(f_i^{st}, 3\pi/4)$ is introduced in (34). Values of the Φ_2^i, S_2, S_2'' function at the additional stationary phase points of the second contour, $f = f_{3,4}^{st}$ are

$$|\Phi_2^{x,y}(f_3^{st}) + \Phi_2^{x,y}(f_4^{st})| = \frac{\left(2(a+b)^2+1\right)|a-b|}{\sqrt{2ab}(a+b)\sqrt{(a+b)^2+1}} = \Phi_{sum}, \tag{A.13}$$

$$\Phi_2^0\left(f_3^{\mathrm{st}}\right) = \Phi_2^0\left(f_4^{\mathrm{st}}\right) = \frac{2(a+b)^2+1}{(a+b)^2+1} = \Phi_{\mathrm{add}}, \tag{A.14}$$

$$S_2''\left(f_{3,4}^{\mathrm{st}}, 3\pi/4\right) = -\frac{(16a^2b^2-(a-b)^2)(1+(a-b)^2))(2(a+b)^2+1)^2}{2\sqrt{ab}(a+b)^3((a+b)^2+1)^{3/2}} = S_3''. \tag{A.15}$$

Notably, when $a \to b$ the second derivative, $S_{1,2}'' \to \pm\infty$ (A.11) and the first two terms in the (A.12) asymptote go to zero. With that $\Phi_3^{x,y} = 0$ and

$$S_1\left(\frac{\pi}{4}, \frac{\pi}{4}\right) + S_2\left(\frac{\pi}{4}, \frac{\pi}{4}\right) = 2S_2\left(f_i^{\mathrm{st}}, \frac{3\pi}{4}\right). \tag{A.16}$$

[a)]Email: kolesnichenko@ilt.kharkov.ua

[1]R. Winkler, *Spin-Orbit Coupling Effects in Two-Dimensional Electron and Hole Systems* (Springer-Verlag, Berlin Heidelberg, 2003).
[2]M. Trushin, K. Výborný, P. Moraczewski, A. A. Kovalev, J. Schliemann, and T. Jungwirth, Phys. Rev. B **80**, 134405 (2009).
[3]D. Bercioux and P. Lucignano, Rep. Prog. Phys. **78**, 106001 (2015).
[4]J. Friedel, Philos. Mag. **43**, 153 (1952).
[5]J. Friedel, Nuovo Cimento **7**, 287 (1958).
[6]A. A. Zvyagin and H. Johannesson, Phys. Rev. Lett. **81**, 2751 (1998).
[7]C. Kittel, *Quantum Theory of Solids* (John Wiley & Sons, Inc., New York, 1963).
[8]H. Gawronski, J. Fransson, and K. Morgenstern, Nano Lett. **11**, 2720 (2011).
[9]P. Mallet, I. Brihuega, V. Cherkez, J. M. Gómez-Rodríguezc, and J. Veuillen, C. R. Phys. **17**, 294 (2016).
[10]C. Bai, *Scanning Tunneling Microscopy and its Applications* (Springer Verlag, New York, 2000).
[11]M. Bode, Rep. Prog. Phys. **66**, 523 (2003).
[12]J. Tersoff and D. R. Hamann, Phys. Rev. Lett. **50**, 1998 (1983).
[13]I. O. Kulik, Yu. N. Mitsai, and A. N. Omel'yanchuk, Sov. Phys.-JETP **39**, 514 (1974) [Zh. Eksp. Theor. Phys. **66**, 1051 (1974)].
[14]Ye. S. Avotina, Yu. A. Kolesnichenko, A. N. Omelyanchouk, A. F. Otte, and J. M. Ruitenbeek, Phys. Rev. B **71**, 115430 (2005).
[15]Ye. S. Avotina, Yu. A. Kolesnichenko, and J. M. van Ruitenbeek, Fiz. Nizk. Temp. **36**, 1066 (2010) [Low Temp. Phys. **36**, 849 (2010)].
[16]D. Wortmann, S. Heinze, Ph. Kurz, G. Bihlmayer, and S. Blügel, Phys. Rev. Lett. **86**, 1998 (2001).
[17]N. V. Khotkevych, N. R. Vovk, and Yu. A. Kolesnichenko, Fiz. Nizk. Temp. **42**, 387–397 (2016) [Low Temp. Phys. **42**, 298 (2016)].
[18]L. Petersen and P. Hedegard, Surf. Sci. **459**, 49 (2000).
[19]N. V. Khotkevych, Yu. A. Kolesnichenko, and J. M. van Ruitenbeek, preprint arXiv:1601.03154 (2016).
[20]Y. Kohsaka, T. Machida, K. Iwaya, M. Kanou, T. Hanaguri, and T. Sasagawa, Phys. Rev. B **95**, 115307 (2017).
[21]V. Kaladzhyan, P. Simon, and C. Bena, Phys. Rev. B **94**, 134511 (2016).
[22]J. Fransson, Phys. Rev. B **92**, 125405 (2015).
[23]S. Lounis, A. Bringer, and S. Blugel, Phys. Rev. Lett. **108**, 207202 (2012).
[24]J. Hutchinson and J. Maciejko, Phys. Rev. B **93**, 245309 (2016).
[25]J. I. Pascual, G. Bihlmayer, Yu. M. Koroteev, H.-P. Rust, G. Ceballos, M. Hansmann, K. Horn, E. V. Chulkov, S. Blügel, P. M. Echenique, and Ph. Hofmann, Phys. Rev. Lett. **93**, 196802 (2004).
[26]O. Pietzsch, S. Okatov, A. Kubetzka, M. Bode, S. Heinze, A. Lichtenstein, and R. Wiesendanger, Phys. Rev. Lett. **96**, 237203 (2006).
[27]A. Stróżecka, A. Eiguren, and J. I. Pascual, Phys. Rev. Lett. **107**, 186805 (2011).
[28]E. I. Rashba, Fiz. Tverd. Tela **2**, 1224 (1960) [Sov. Phys. Solid State **2**, 1109 (1960)].
[29]Yu. Bychkov and E. I. Rashba, JETP Lett. **39**, 78 (1984).
[30]G. Dresselhaus, Phys. Rev. **100**, 580 (1955).
[31]S. D. Ganichev and L. E. Golub, Phys. Status Solidi B **251**, 1801 (2014).
[32]S. M. Badalyan, A. Matos-Abiague, G. Vignale, and J. Fabian, Phys. Rev. B **81**, 205314 (2010).
[33]D. H. Berman and M. E. Flatté, Phys. Rev. Lett. **105**, 157202 (2010).
[34]E. G. Mishchenko and B. I. Halperin, Phys. Rev. B **68**, 045317 (2003).
[35]G. A. Korn, *Mathematical Handbook for Scientists and Engineers* (Nauka, Moscow, 1974).
[36]L. D. Landau, *Quantum Mechanics: Nonrelativistic Theory* (Nauka, Moscow, 1989).
[37]D. H. Berman and M. E. Flatté, Proc. SPIE **8100**, 810014 (2011).
[38]I. M. Lifshits, M. Ya. Azbel', and M. I. Kaganov, *Electron Theory of Metals* (Consultants Bureau, New York, 1973).
[39]A. M. Kosevich, Fiz. Nizk. Temp. **11**, 1106 (1985) [Sov. J. Low Temp. Phys. **11**, 611 (1985)].
[40]N. V. Khotkevych-Sanina, Yu. A. Kolesnichenko, and J. M. van Ruitenbeek, New J. Phys. **15**, 123013 (2013).
[41]M. V. Fedoryuk, *Method of Steepest Descent* (Nauka, Moscow, 1977).

This article was published in English in the original Russian journal. Reproduced here with stylistic changes by AIP Publishing.